Applied Catalysis B: Environmental 95 (2010) 393–399

Contents lists available at ScienceDirect

Applied Catalysis B: Environmental

journal homepage: www.elsevier.com/locate/apcatb

Photocatalytic performance of tetragonal and cubic β-In_2S_3 for the water splitting under visible light irradiation

Xianliang Fu [a], Xuxu Wang [a,*], Zhixin Chen [a], Zizhong Zhang [a], Zhaohui Li [a], Dennis Y.C. Leung [b], Ling Wu [a], Xianzhi Fu [a]

[a] Research Institute of Photocatalysis, Fuzhou University, Fuzhou 350002, China
[b] Department of Mechanical Engineering, The University of Hong Kong, Hong Kong, China

ARTICLE INFO

Article history:
Received 14 October 2009
Received in revised form 9 January 2010
Accepted 20 January 2010
Available online 25 January 2010

Keywords:
In_2S_3
Photocatalytic activity
Hydrogen evolution
Vacancy

ABSTRACT

Tetragonal (T-In_2S_3) and cubic (C-In_2S_3) β-In_2S_3 were synthesized by hydrothermal method. The obtained products were characterized by X-ray diffraction (XRD), diffuse reflectance spectra (DRS), X-ray photoelectron spectroscopy (XPS), and transmission electron microscopy (TEM) technologies. Their photocatalytic activity for hydrogen evolution from water under visible light irradiation ($\lambda > 400$ nm) was evaluated. It was revealed that the photocatalytic activity of β-In_2S_3 was strongly affected by the arrangement characteristic of the indium vacancies. The vacancy ordered T-In_2S_3 showed no activity for hydrogen production, while the vacancy disordered C-In_2S_3 exhibited stable activity. For C-In_2S_3 sample, further studies indicated that the photoactivity strongly depended on the nature and the amount of noble metal cocatalyst. The optimum loading value of Pt cocatalyst was found to be 2 wt.%. With this loading amount as a reference value, the hydrogen production rate of noble-metal-loaded C-In_2S_3 decreased in the order Pd > Pt > Ru > Au/C-In_2S_3.

1. Introduction

Photocatalytic production of hydrogen from water is an attractive and challenging issue in the conversion of solar energy into chemical energy [1,2]. As a means to achieve this goal, many oxide-based photocatalysts have been developed [3]. Unfortunately, most of them, such as $SrTiO_3$ [4], $NaTaO_3$ [5], and $K_4Nb_6O_{17}$ [6], are wide-band-gap semiconductors and only active under UV light irradiation, which accounts for only about 5% of the solar spectrum. From the viewpoint of the utilization of solar light energy, it is indispensable to develop the photocatalyst capable of using visible light, which accounts for 45% of solar energy. Although some In and S-based ternary chalcogenide photocatalysts, such as $ZnIn_2S_4$ [7,8], $CdIn_2S_4$ [9], $CuInS_2$ [10], and $AgInS_2$ [10] have been developed for this purpose in the past few years, studies on the photocatalytic activity of indium sulfide, which directly formed from these two elements, has seldom been reported. As one kind of mid band gap semiconductors, indium sulfide is a potential material for hydrogen production from water under sunlight irradiation.

Generally, indium sulfide has two kinds of composition forms, InS and In_2S_3, with band gaps of 2.44 eV [11] and 2.0–2.2 eV [12], respectively. Between these two compounds, most of the research works have been focused on In_2S_3. At atmospheric pressure, In_2S_3 is known to crystallize in three different structural forms [13], i.e., α-In_2S_3 (defect cubic structure), β-In_2S_3 (defect spinel structure obtained in either cubic or tetragonal form), and γ-In_2S_3 (layered hexagonal structure). Among these three forms, β-In_2S_3 has received extensive attention over the past decades because of its defect structure and corresponding optical, acoustic and electronic properties. Based on these properties, the applications of β-In_2S_3 have been developed in many areas, such as the preparation of green or red phosphors for color televisions [14], photocatalytic degradation of dyes [15,16], and as the buffer layer instead of toxic CdS in $CuInSe_2$ and $CuInS_2$-based solar cells [17]. Although there are some reports [3,18–20] about the photocatalytic activities of β-In_2S_3 for hydrogen evolution, the studies are still limited and the results are somewhat conflicting. Some studies [3,20,21] suggested that In_2S_3 did not catalyze photochemical water splitting, whereas other studies [18,19] indicated it did occur. The intrinsic reason for this discrepancy has never been attempted to be clarified. An effort to address this issue will be helpful not only in the understanding of the photoactivity of these In-based ternary chalcogenide, but also in the developing of a novel photocatalyst based on these In-containing chalcogenide.

In the present work, tetragonal (T-In_2S_3) and cubic (C-In_2S_3) β-In_2S_3 samples were synthesized via different hydrothermal method and their photocatalytic activities for hydrogen evolution were then compared under visible light irradiation ($\lambda > 400$ nm). The results showed that the indium vacancy ordered T-In_2S_3

* Corresponding author. Tel.: +86 591 83779251; fax: +86 591 83779251.
E-mail address: xwang@fzu.edu.cn (X. Wang).

0926-3373/$ – see front matter © 2010 Elsevier B.V. All rights reserved.
doi:10.1016/j.apcatb.2010.01.018

showed no activity for hydrogen generation, while the vacancy disordered C-In_2S_3 exhibited stable photoactivity. The differences of their crystal structure account for the different activities. For C-In_2S_3 sample, the effects of the loaded Pt amount and the nature of the cocatalyst (Pd, Pt, Au, and Ru) on the rate of hydrogen evolution were further investigated.

2. Experimental

2.1. Preparation and characterization of T-In_2S_3 and C-In_2S_3

All of the reagents were analytical grade and used without further purification. Both T-In_2S_3 and C-In_2S_3 were synthesized according to modified hydrothermal methods which had been reported by our groups [22,23] and Naik et al. [18], respectively. For T-In_2S_3 sample, 2 mmol $InCl_3{\cdot}4H_2O$ and 6 mmol thioacetamide (CH_3CSNH_2) were used as the precursors. The reagents were first dissolved in 50 mL water in a Teflon liner with 100 mL capacity, and then the solution pH was adjusted to 2.5 by adding hydrochloric acid. At last the Teflon liner was sealed in a stainless steel autoclave and maintained at 160 °C for 6 h. If 1 mL $CuCl_2$ solution (0.092 M) was added to the reaction solution prior to the hydrothermal treatment, 1.0 wt.% Cu containing T-In_2S_3 sample (Cu 1.0 wt.%/In_2S_3, theoretical value) could be obtained. As for the C-In_2S_3 sample, 4.5 mmol $In(NO_3)_3$ and 13.5 mmol thiourea (NH_2CSNH_2) were first dissolved in 80 mL deionized water in the Teflon liner. Then the liner was sealed in the autoclave and maintained at 160 °C for 60 h. After cooling to room temperature, both the precipitates of T-In_2S_3 and C-In_2S_3 were collected, washed with distilled water and absolute ethanol several times, and finally dried in air at 60 °C.

X-ray diffraction (XRD) patterns of the samples were collected on a Bruker D8 Advance X-ray diffractometer with Ni filtered Cu Kα radiation (λ = 1.5406 Å). The accelerating voltage and the applied current were 40 kV and 40 mA, respectively. The UV–vis diffuse reflectance spectra (UV–vis DRS) were recorded on a Varian Cary 500 Scan UV–vis-NIR spectrometer with $BaSO_4$ as a reference sample. The BET surface areas were determined by nitrogen adsorption-desorption on the Micromeritics ASAP 2020. Transmission electron microscopy (TEM) and high-resolution TEM (HRTEM) images were obtained by a JEOL model JEM 2010 EX instrument at an accelerating voltage of 200 kV. X-ray photoelectron spectroscopy (XPS) analysis was conducted on an ESCALAB 250 photoelectron spectroscopy (Thermo Fisher Scientific) at 3.0×10^{-10} mbar using Al Kα X-ray beam (1486.6 eV). All binding energies were referenced to the C 1s peak of the surface adventitious carbon at 284.8 eV.

2.2. Photocatalytic activity measurements

Photocatalytic hydrogen evolution reactions were performed in a closed gas-recirculation system equipped with an external-irradiation reaction cell made of Pyrex glass. In a typical run, 50 mg photocatalyst was suspended in 170 mL 0.025 M Na_2S and 0.025 M Na_2SO_3 mixed solution by magnetic stirring. Then 1 mL H_2PtCl_6 solution (containing 1 mg Pt) was added to the suspension. Pt was photodeposited onto the surface of In_2S_3 in situ during the initial photocatalytic reaction [24]. Prior to the reaction, the system was evacuated by a mechanical pump and then filled with 101 kPa of high-purity N_2 (>99.99%). This process was repeated three times in order to remove O_2 in the system, which had been shown to be a powerful inhibitor for photocatalytic hydrogen production [25]. The suspension was then irradiated from the flat side face of the reactor by a 300 W Xe lamp with a cut-off filter (λ > 400 nm). The temperature of the reaction solution was controlled at about 35 °C by air conditioner. The evolved hydrogen gas was circulated with a micro diaphragm gas pump in the system (NMP-830KNE, KNF Neuberger, Germany) and its amount was determined by an online gas chromatograph (GC112A, Shanghai Precision Scientific Instrument Co., Ltd., TCD, N_2 carrier).

2.3. Measurement of the photoinduced electron-transfer process in photoirradiated β-In_2S_3 (T-In_2S_3 and C-In_2S_3)

Methyl viologen (MV^{2+}) hydrate (Alfa, 98%) was used as a photoinduced-electron trap. It can be reduced by the photogenerated electrons to form $MV^{\bullet+}$. The absorption peaks at ca. 400 and 610 nm were characteristics of $MV^{\bullet+}$ and served as a probe to trace the photoinduced charge-transfer process [26]. The measurement reactions were performed in aqueous solution due to MV^{2+} can be directly reduced to $MV^{\bullet+}$ by the sacrificial agent of Na_2S and Na_2SO_3 mixed solution (see Supplementary data, Fig. S1), which will hamper the observation of charge-transfer process of β-In_2S_3. So no Na_2S and Na_2SO_3 were used as sacrificial hole scavengers. At first 0.9 mg of β-In_2S_3 (T-In_2S_3 or C-In_2S_3) was suspended in 2.8 mL 1.0×10^{-3} M MV aqueous solution in a colorimeter cell by magnetic stirring, and then, after purging of high-purity N_2 for 10 min, the suspension was irradiated by a spot light source (Hamamatsu Co., LC8, equipped with a 400 nm filter) still under the purging condition. After illuminating for various periods, the absorbance of the solution was measured by a Varian UV–vis spectrophotometer (Cary-50).

3. Results and discussion

3.1. Spectroscopic characterization

Fig. 1 depicts the XRD patterns of the as-prepared T-In_2S_3 and C-In_2S_3 samples. The corresponding spectrum of T-In_2S_3 showed that all the diffraction peaks can be indexed to tetragonal β-In_2S_3 (JCPDS 25-0390). No other impurities, such as In_2O_3, InS or $In(OH)_3$, were detected, indicating the pure phase of the sample. While the pattern of C-In_2S_3 can be assigned to cubic β-In_2S_3 with lattice parameter of a = 10.73 Å (JCPDS 32-0456). Compared with T-In_2S_3 sample, the higher background noise and the broader diffraction peaks of C-In_2S_3 indicated that the sample was not well crystallized.

In addition to the crystal structure, the optical properties of the as-prepared two samples were also compared, as shown in Fig. 2. Two absorption thresholds at 613 and 620 nm were observed for T-In_2S_3 and C-In_2S_3 samples, respectively, which corresponded to band gap energies of 2.03 and 1.98 eV. These values are almost consistent with the reported bulk In_2S_3 value of 2.07 eV [11].

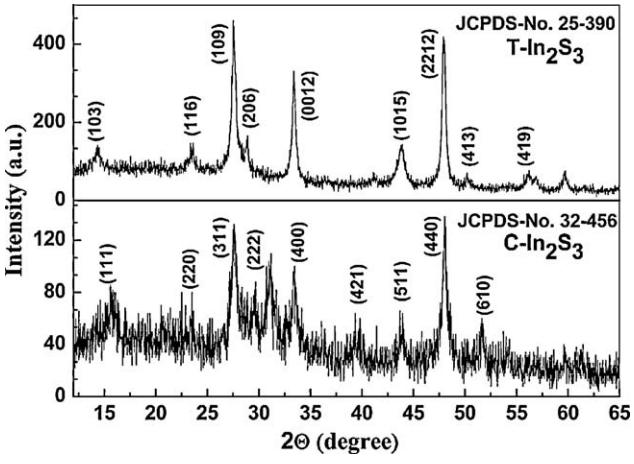

Fig. 1. XRD patterns of the as-prepared T-In_2S_3 and C-In_2S_3 samples.

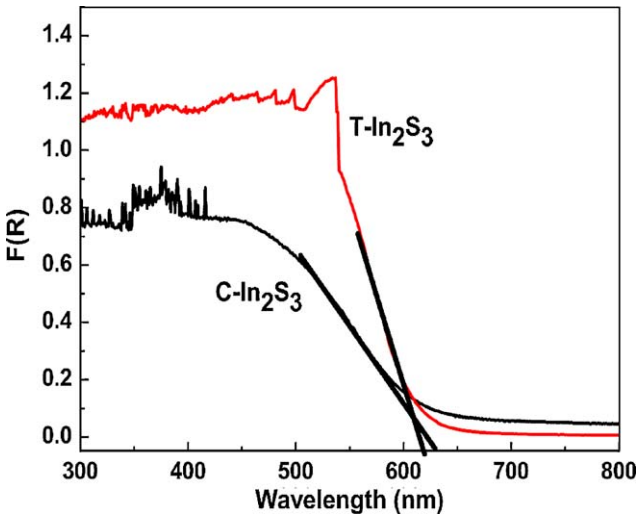

Fig. 2. UV–vis diffuse reflectance spectrum of T-In_2S_3 and C-In_2S_3 samples.

Obviously, T-In_2S_3 sample showed higher visible light absorption ability than C-In_2S_3 sample.

To further investigate the surface compositions and chemical state of the as-prepared In_2S_3 products, XPS measurements were carried out. The XPS spectra of T-In_2S_3 and C-In_2S_3 samples were similar (Supplementary data, Fig. S2) and consistent with the typical In_2S_3 spectrum reported by other researchers [27]. The typical survey spectrum of C-In_2S_3 (fresh) is shown in Fig. 3a. It reveals that no peaks of other elements except In, S, O, and C were observed. The peaks of C and O probably came from the absorbed gaseous molecules and the oxidation of samples, respectively. High resolution core spectrum for In 3d, S 2p of fresh C-In_2S_3 are displayed in Fig. 3b and c. The peaks at the binding energy value of 445 and 452.5 eV were related to In $3d_{5/2}$ and In $3d_{3/2}$, while the peaks at 161.3 and 162.5 eV could be attributed to S $2p_{3/2}$ and S 2p transition, respectively. The observed binding energy values of In 3d and S 2p agreed well with the reported data for In_2S_3 [27,28]. The In and S spin orbit separations were found to be 7.5 and 1.2 eV, and the ratios of two peak areas were ca. 2:3 and 1:2. These results indicated that the In and S were present as In^{3+} and S^{2-} in the samples.

It is known that the S-based photocatalysts are prone to undergo photocorrosion during the photocatalytic reaction [29]. Thus, in order to determine whether the photocorrosion reaction was occurred, the used C-In_2S_3 sample which showed stable activity for hydrogen evolution (vide infra, Fig. 5) was also investigated by XPS after 10 h of reaction time and compared with the fresh one. As Fig. 3a shows that the survey spectrum of used C-In_2S_3 was almost identical to the fresh one. No S^0 product (S 2p of S^0 peak at 164.2 eV [29]) was confirmed by the core spectrum of S 2p (Fig. 3d) implying that the photocorrosion was not apparent after 10 h hydrogen evolution reaction.

3.2. Morphology

The morphologies and the structures of the prepared In_2S_3 samples were examined using TEM, HRTEM, and Electron diffraction (ED) measurements. As shown in Fig. 4A (a) and B (a), both T-In_2S_3 and C-In_2S_3 were of nano-flake structure. The HRTEM image (Fig. 4A (b)) of T-In_2S_3 sample reveals that the lattice spacing of the flake was about 0.32 nm, which could be assigned to the (1 0 9) planar spacing of tetragonal β-In_2S_3. While for the C-In_2S_3 sample, two interplanar distance of 0.38 and 0.62 nm were observed, corresponding to the (2 2 0) and (1 1 1) planar spacing of cubic β-In_2S_3, respectively (Fig. 4B (b and c)). The presence of the diffraction rings in ED patterns (Fig. 4A (c) and B (d)) demonstrate that both the two samples were polycrystalline. The bright and sharp ED pattern of T-In_2S_3 indicates that this sample had better crystallinity than C-In_2S_3. The interplanar distance values corresponding to the diffraction rings of T-In_2S_3 sample were 7.45, 6.41, 3.77, 3.22, 2.47, and 2.25 Å (from the inner to the outer), which could be assigned to the planes (1 0 1), (1 0 3), (1 1 6), (1 0 9), (3 0 3), and (3 0 7) of the tetragonal β-In_2S_3, respectively. For C-In_2S_3 sample, ED reflection rings of (1 1 1), (2 1 1), (4 2 1) and (5 1 1) planes of cubic β-In_2S_3 were observed. Therefore, by means of the ED technique, the phase identifications which had been made with the XRD results were further confirmed. The energy dispersive X-ray analysis (EDX) results (Fig. 4A (d) and B (e)) suggest that the products were composed of S and In, and the ratios of sulfur to indium atoms were 1.63 and 1.48 for T-In_2S_3 and C-In_2S_3, respectively. These values are close to the theoretical value of 1.5 expected for In_2S_3.

3.3. Photocatalytic activity test

3.3.1. Comparison of hydrogen production activities between T-In_2S_3 and C-In_2S_3

The photocatalytic activities of T-In_2S_3 and C-In_2S_3 were investigated by photocatalytic production of hydrogen from Na_2S and Na_2SO_3 mixed aqueous solution under visible light

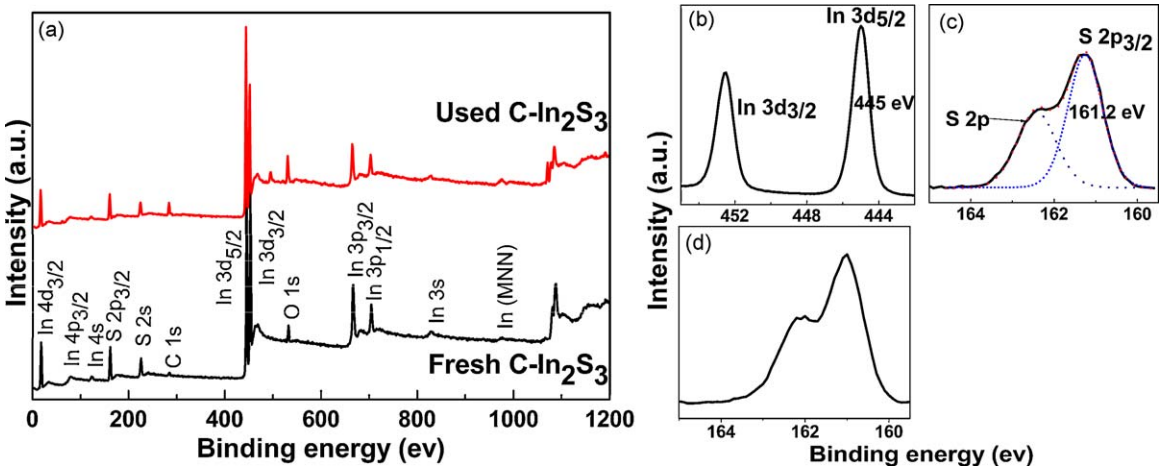

Fig. 3. (a) XPS survey spectra of fresh and used C-In_2S_3; (b) In 3d and S 2p XPS spectrum of fresh C-In_2S_3 and S 2p, Pt 4f spectrum of used C-In_2S_3.

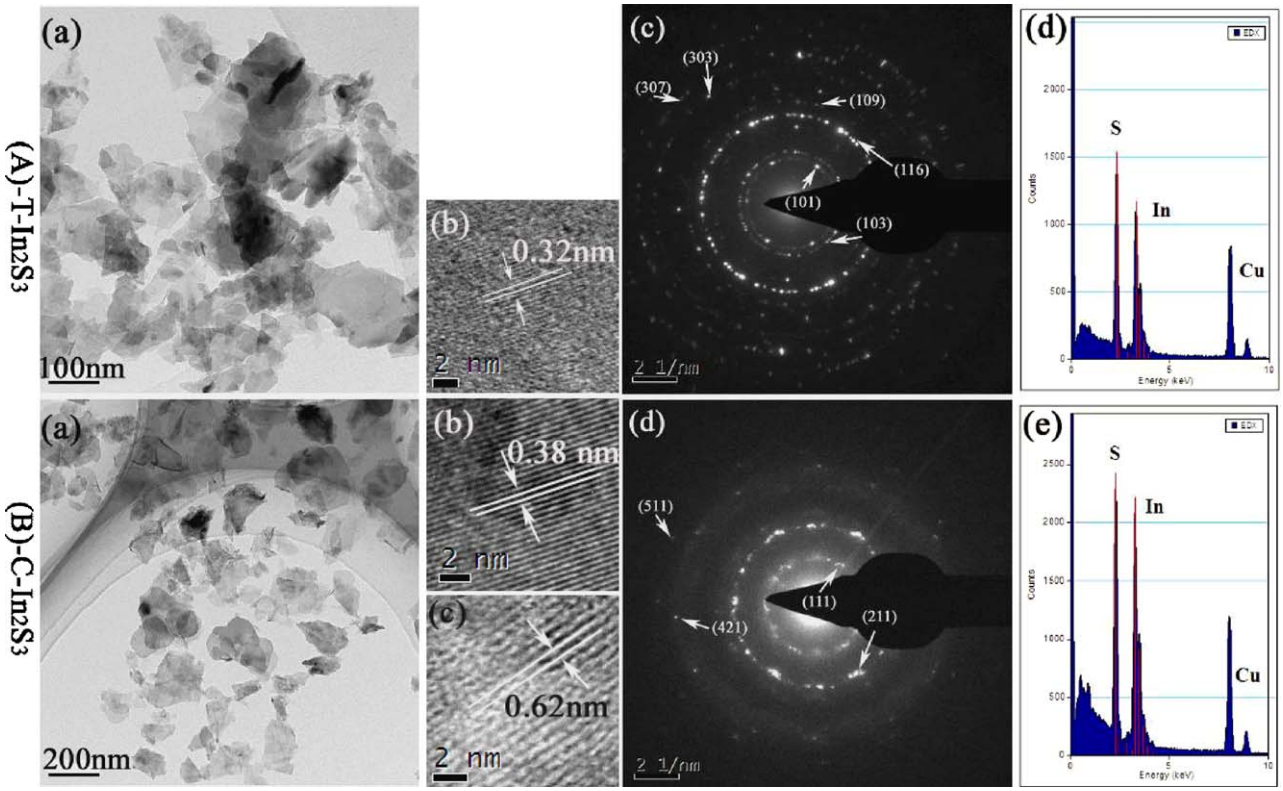

Fig. 4. (A): (a) TEM, (b) HRTEM images and corresponding (c) ED and (d) EDX patterns of T-In_2S_3 sample; (B) (a) TEM, (b and c) HRTEM images and corresponding (d) ED and (e) EDX patterns of C-In_2S_3 sample

irradiation ($\lambda > 400$ nm) (Fig. 5). 2.0 wt.% of Pt was loaded as a cocatalyst to improve the hydrogen production efficiency by in situ photochemical deposition method [24]. A blank experiment revealed that no hydrogen was produced without an In_2S_3 sample. It was surprising to note that T-In_2S_3 sample which was well-crystallized and had a strong ability to absorb visible light showed no activity for hydrogen production, even after 10 h irradiation. However, for C-In_2S_3, the poor-crystallized and low ability to absorb visible light sample, the amount of evolved hydrogen was almost linearly increased with the increase of irradiation time and the average hydrogen generation rate was calculated to be 36 μmol h^{-1} (50 mg). The hydrogen producing ability of cubic β-In_2S_3 had also been observed by Shen and Guo [19], but the ability of tetragonal type sample had not been investigated by them. Recently, Naik et al. [18] found that the cubic sample showed a 33% higher photoactivity for hydrogen production than of tetragonal β-In_2S_3 by H_2S splitting reaction, an easier occurred reaction than H_2O splitting.

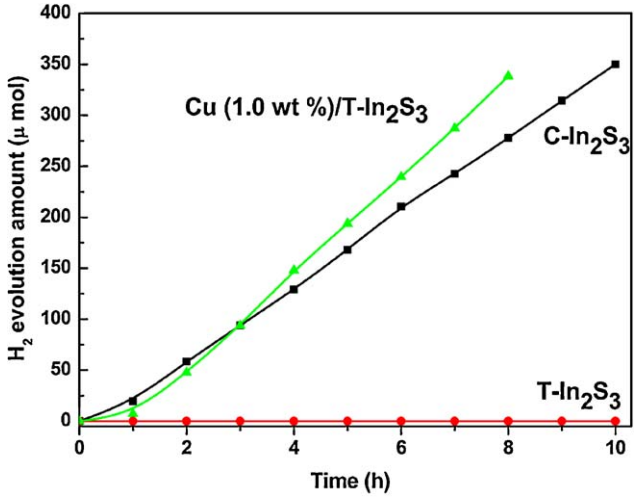

Fig. 5. Photocatalytic hydrogen evolution from 170 mL Na_2S (0.025 M) and Na_2SO_3 (0.025 M) mixed aqueous solution suspended with the Pt 2.0 wt.%/T-In_2S_3 or Pt 2.0 wt.%/C-In_2S_3 powder photocatalysts (50 mg) under 300 W Xe lamp irradiation ($\lambda > 400$ nm).

The results of our present work bring up a question as to why T-In_2S_3 and C-I_2S_3 show such a significant difference in their photocatalytic activities for water splitting to generate hydrogen. Generally, four factors are supposed [3] to influence the photocatalytic activity of hydrogen production, including the crystal morphology, specific surface area, crystallinity, and crystal structure of the photocatalyst. Some particular morphology, such as the nanostep structure of $NaTaO_3$ [5] and CdS [30], can separate the H_2 and O_2 formation sites and therefore can enhance the hydrogen production rate. In addition, as demonstrated in the case of $CdIn_2S_4$ [9], $Sr_3Ti_2O_7$ [31] and $HLaNb_2O_7$ [32], photocatalysts with high specific surface area or high crystallinity can generally lead to higher photocatalytic activity for hydrogen production. In our case, both T-In_2S_3 and C-I_2S_3 take nano-flake morphology (Fig. 4), and therefore morphology cannot account for the activity discrepancy. Although the BET surface area of the well crystallized T-In_2S_3 (34.2 m^2/g) is smaller than that of C-In_2S_3 (44.3 m^2/g), it is also hard to attribute the great discrepancy to the differences in surface area or crystallinity of the two samples. So we expect that the differences of their crystal structure may well account for the activity discrepancy.

The β phase In_2S_3 crystallizes in a defect spinel structure. Contrary to the normal spinel structure, one third of the tetrahedral sites are empty, which leads to the quasi-quaternary compound formula: $[In_6]_{Oh}[In_2\square]_{Td}S_{12}$ (□ is the vacant sites. Td and Oh represent the tetrahedral and octahedral sites, respectively) [33]. The arrangement characteristic of the cation vacancies

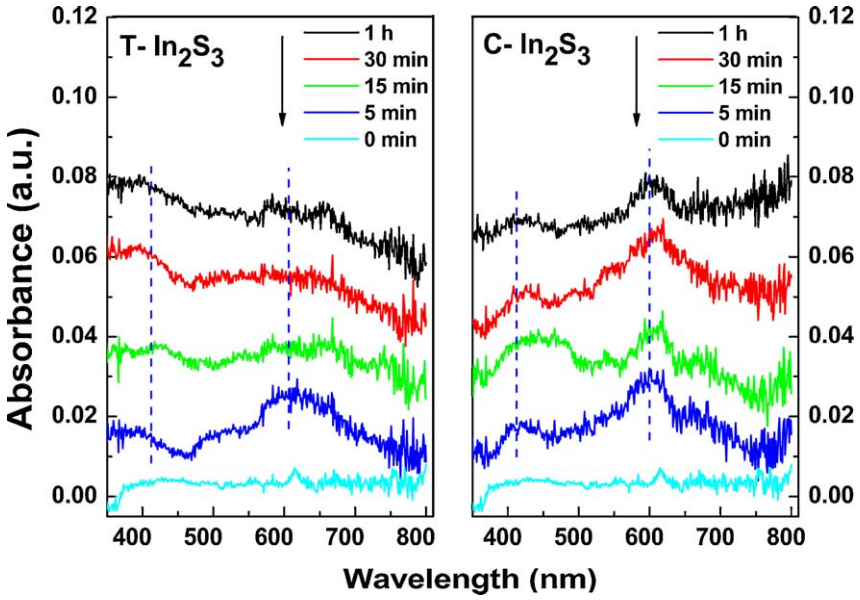

Fig. 6. Absorption spectra of $MV^{\bullet+}$ radical generated over T-In_2S_3 and C-In_2S_3 sample as a function of exposure time.

determines which product, T-In_2S_3 or C-In_2S_3, will be obtained. If the vacancies are ordered on tetrahedral cation sites, the resulted sample will be T-In_2S_3. As a result of the ordering, the cubic symmetry of spinel structure is subsequently lost and a new tetragonal supercell is formed, which contains three spinel blocks along the *c*-axis. While if the vacancies presented in a random arrangement, C-In_2S_3 sample will be obtained and has a cubic defect spinel structure [34].

Active photocatalysts are generally found [3] to have efficient charge-transport pathways which connect the interior with the surface of the photocatalyst where water splitting reaction occurs. For oxide semiconductors, oxide-bridged metal ions are assumed to play this role [3]. According to this assumption, we proposed that sulfur-bridged indium ions should play a similar role to transfer the photogenerated charges. However, the transportation efficiency of the pathway will be depressed by the presence of indium vacancies. For the T-In_2S_3 sample, the three-dimensional defect structure resulted from the ordering of indium vacancies will further discourage the migration of photoinduced charges [20] and, as a consequence, shows virtually no activity for hydrogen evolution in Fig. 5. However, C-In_2S_3 sample has not this structure defect and the charges transportation efficiency is only affected by the absence of the indium cations, and thus can exhibit some measurable activity for hydrogen evolution. In Naik et al.'s research [18], they also thought that the crystal structure is partially accounted for the photoactivity difference of cubic and tetragonal β-In_2S_3 but gave no further explanation.

The photoinduced charge-transfer process of T-In_2S_3 and C-In_2S_3 sample was studied by observing the absorption spectra of $MV^{\bullet+}$ radicals, which resulted from the reduction of MV^{2+} by photoinduced electrons.

$$MV^{2+} + e \rightarrow MV^{\bullet+} \quad (1)$$

As shown in Fig. 6, the solution showed no apparent absorbance before turn on the spot light. After irradiating for 5 min, an absorbance peak around 600 nm was observed for T-In_2S_3 sample, but with the exposure time increased, the peak became obscure and almost disappeared 15 min later. This phenomenon suggests that, for T-In_2S_3 sample, the $MV^{\bullet+}$ radicals can only be formed in the initial irradiation stage, and afterwards they are consumed in some way, such as transforming to $(MV^{\bullet+})_2$ [35]. However, compared to T-In_2S_3, the peaks intensities of $MV^{\bullet+}$ formed over C-In_2S_3 showed no significant changes during the observation time.

Because the measurement reactions were performed in aqueous solution, with reaction (1) proceed, the surface of In_2S_3 (T-In_2S_3 or C-In_2S_3) would be oxidized by the cumulated photoexcited holes and then no electrons could be generated on the surface. If the thickness of the inactive surface layer is not too large, the light can still penetrate into a deep interior of the sample and some electrons can be generated there. In this case, the reduction efficiency of MV^{2+} would highly depend on the number of excited electrons which transferred from interior to the surface. If the electrons were hard to get to the surface, the concentration of $MV^{\bullet+}$ would subsequently decreased because of some extinction reactions. Thus the variation of $MV^{\bullet+}$ concentration with the irradiation time can be used to asses the movability of excited electrons formed in the interior of the sample. Therefore, according to the result shown in Fig. 6, it is not difficult to deduce that, for T-In_2S_3 sample, the photogenerated electrons are truly difficult to move from interior to the surface. This property is the reason why T-In_2S_3 shows no photoactivity for H_2 evolution in Fig. 5. However, for C-In_2S_3 sample, the peak intensities of $MV^{\bullet+}$ have not changed

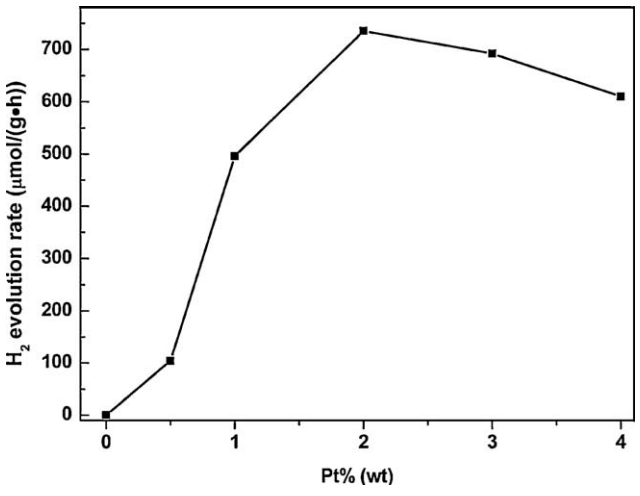

Fig. 7. The effect of Pt content on the hydrogen evolution rate of Pt/C-In_2S_3.

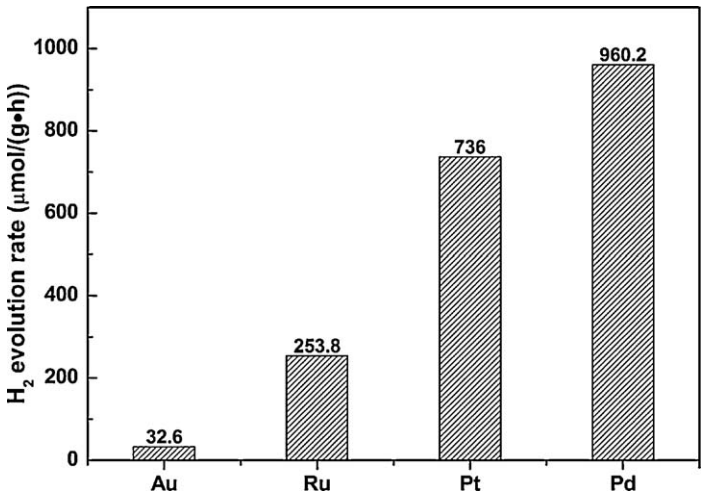

Fig. 8. Comparison of hydrogen evolution among different noble-metal-loaded C-In_2S_3.

very much (indicating an equilibrium between the production and the extinction of $MV^{\bullet+}$) during the first 30 min illumination time, suggesting the generated electrons can move from interior to its surface and therefore shows stable activity for hydrogen evolution in Fig. 5. After another 30 min illumination, the concentration has somewhat decreased. It is reasonable because, with the illumination time prolonged, the thickness of inactive surface layer will further increased, which reduces the amount of light penetrated into the deep interior of C-In_2S_3.

The cation vacancies of β-In_2S_3 can be filled either by replacing the tetrahedral In atoms (including the vacancy sites) with other metals, such as Zn, Cd, or directly with external elements of Cu [36,37] and the photocatalytic activity of the resulted samples should be substantially improved. For the first approach, the resulted samples are $[In_6]_{Oh}[Zn_3]_{Td}S_{12}$ or $[In_6]_{Oh}[Cd_3]_{Td}S_{12}$, (i.e. $ZnIn_2S_4$ or $CdIn_2S_4$), and the prediction has already been extensively verified by the reported results [7,9,18]. For the second approach, the resulted sample is Cu containing T-In_2S_3, and the prediction is also partially confirmed by our observation as shown in Fig. 5. The primary result indicated that the photoactivity of T-In_2S_3 which has shown no activity for hydrogen production can be significantly improved by adding 1.0 wt.% of Cu element to the sample. Further works are in progress in our laboratory to systemically assess the effect of the Cu containing on the photoactivity of β-In_2S_3, including C-In_2S_3 sample.

3.3.2. *Factors affecting photocatalytic activity of C-In_2S_3*

At last, the effect of some factors on the H_2 production of C-In_2S_3 sample was further investigated. The factors include the loading amount of cocatalyst (Pt) and the nature of the cocatalyst. As shown in Fig. 7 (see Supplementary data, Fig. S3), the hydrogen evolution rate was greatly enhanced by increasing Pt content from 0 to 2.0 wt.% and reached a maximum (736 μmol g^{-1} h^{-1}) at ca. 2.0 wt.%. Further increasing the amount from 2.0 wt.% to 4.0 wt.%, the hydrogen evolution rate was slightly reduced. The appearance of a maximum in activity with an optimum loading of cocatalyst has also been observed for other photocatalysts loaded with Pd [38] or Ru [39]. Without the cocatalyst Pt, there was only trace amount of hydrogen evolved (0.034 mL, 10 h) and the color of the C-In_2S_3 turned from orange to dark red due to the undesirable photocorrosion. Therefore, the cocatalyst of Pt is indispensable to avoid the decomposition of In_2S_3, even in the presence of the sacrificial agents of Na_2S and Na_2SO_3.

Except of Pt, some other noble metals, such as Pd, Ru, and Au were also used as the cocatalyst. The feed solutions for them were $PdCl_2$, $RuCl_3$, and $HAuCl_4$ aqueous solution, respectively (1 mg metal/mL). When loaded with 2.0 wt.% of these noble metals, the photoactivities of bare C-In_2S_3 were significantly improved (see Supplementary data, Fig. S3) and the hydrogen evolution rates decreased in the order of Pd (960.2) > Pt (736) > Ru (253.8) > Au/C-In_2S_3 (32.6 μmol h^{-1} g^{-1}) (Fig. 8). A similar order has been observed in our previous study on the photocatalytic reforming of glucose to generate hydrogen over noble-metal loaded TiO_2 [25]. The reasons for the enhancement can be well understood from both the electrochemical principle and the electron structure of the cocatalysts. Due to the low activation potentials for hydrogen evolution, noble metals are often served as the active sites for hydrogen generation and can make hydrogen easy to evolve. Moreover, loading with noble metals can promote the separation of photoexited electrons and holes and this ability is directly related to the value of the noble-metals' work functions [40]. A metal with a large work function, such as Pd and Pt (5.65 and 5.55 eV, respectively [41]), commonly shows the prominent effect and greatly enhances the photocatalytic activity.

4. Conclusions

Nanoflake tetragonal (T-In_2S_3) and cubic (C-In_2S_3) β-In_2S_3 samples were successfully synthesized via hydrothermal method and their photocatalytic property for water splitting to generate hydrogen was determined under visible light irradiation. The results indicated that the photocatalytic activity of β-In_2S_3 is strongly influenced by the sample's crystal structure. The vacancy ordered T-In_2S_3 sample showed virtually no activity for hydrogen production, whereas the vacancy disordered C-In_2S_3 sample exhibited stable activity. The photoactivity of C-In_2S_3 can be significantly improved by loading with large work function of noble metals, such as Pd and Pt. For Pt modified C-In_2S_3, the optimum loading amount of Pt was found to be 2 wt.%.

Acknowledgements

This work is financially supported by the National Natural Science Foundation of China (Grant Nos. 20537010, 20673020, and 28873022), 863 Specialize Program (2008AA06Z326), and the National Basic Research Program of China 973 Program (Grant No. 2007CB613306). The partial supported from the Hong Kong RGC (HKU 7150/05E) is also acknowledged. Thanks program for New Century Excellent Talents in Fujian province (XSJRC2007-19).

Appendix A. Supplementary data

Supplementary data associated with this article can be found, in the online version, at doi:10.1016/j.apcatb.2010.01.018.

References

[1] Z.G. Zou, J.H. Ye, K. Sayama, H. Arakawa, Nature 414 (2001) 625–627.
[2] A. Kudo, Y. Miseki, Chem. Soc. Rev. 38 (2009) 253–278.
[3] F.E. Osterloh, Chem. Mater. 20 (2008) 35–54.
[4] B. Zieliñska, E. Borowiak-Palen, R.J. Kalenczuk, Int. J. Hydrogen Energy 33 (2008) 1797–1802.
[5] H. Kato, K. Asakura, A. Kudo, J. Am. Chem. Soc. 125 (2003) 3082–3089.
[6] M.C. Sarahan, E.C. Carroll, M. Allen, D.S. Larsen, N.D. Browning, F.E. Osterloh, J. Solid State Chem. 181 (2008) 1678–1683.
[7] Z. Lei, W. You, M. Liu, G. Zhou, T. Takata, M. Hara, K. Domen, C. Li, Chem. Commun. 9 (2003) 2142–2143.
[8] S. Shen, L. Zhao, L. Guo, Int. J. Hydrogen Energy 33 (2008) 4501–4510.
[9] B.B. Kale, J.O. Baeg, S.M. Lee, H. Chang, S.J. Moon, C.W. Lee, Adv. Funct. Mater. 16 (2006) 1349–1354.
[10] I. Tsuji, H. Kato, A. Kudo, Angew. Chem. Int. Ed. 44 (2005) 3565–3568.
[11] T. Nishino, Y. Hamakawa, Jpn. J. Appl. Phys. 16 (1977) 1291–1300.
[12] A. Timoumi, H. Bouzouita, M. Kanzari, B. Rezig, Thin Solid Films 480–481 (2005) 124–128.
[13] R. Diehl, R. Nitsche, J. Cryst. Growth 28 (1975) 306–310.
[14] W. Chen, J.-O. Bovin, A.G. Joly, S. Wang, F. Su, G. Li, J. Phys. Chem. B 108 (2004) 11927–11934.
[15] W. Du, J. Zhu, S. Li, X. Qian, Cryst. Growth Des. 8 (2008) 2130–2136.
[16] Y. He, D. Li, G. Xiao, W. Chen, Y. Chen, M. Sun, H. Huang, X. Fu, J. Phys. Chem. C 113 (2009) 5254–5262.
[17] E. Dalas, S. Sakkopoulos, E. Vitoratos, G. Maroulis, L. Kobotiatis, J. Mater. Sci. 28 (1993) 5456–5460.
[18] S.D. Naik, T.C. Jagadale, S.K. Apte, R.S. Sonawane, M.V. Kulkarni, S.I. Patil, S.B. Ogale, B.B. Kale, Chem. Phys. Lett. 452 (2008) 301–305.
[19] S. Shen, L. Guo, J. Solid State Chem. 179 (2006) 2629–2635.
[20] A. Kudo, A. Nagane, I. Tsuji, H. Kato, Chem. Lett. (2002) 882–883.
[21] E.N. Savinov, Y.A. Gruzdkov, V.N. Parmon, Int. J. Hydrogen Energy 14 (1989) 1–9.
[22] Z. Chen, D. Li, W. Zhang, Y. Shao, T. Chen, M. Sun, X. Fu, J. Phys. Chem. C 113 (2009) 4433–4440.
[23] Z. Chen, D. Li, W. Zhang, C. Chen, W. Li, M. Sun, Y. He, X. Fu, Inorg. Chem. 47 (2008) 9766–9772.
[24] M.C. Hidalgo, M. Maicu, J.A. Navio, G. Colon, Catal. Today 129 (2007) 43–49.
[25] X. Fu, J. Long, X. Wang, D.Y.C. Leung, Z. Ding, L. Wu, Z. Zhang, Z. Li, Int. J. Hydrogen Energy 33 (2008) 6484–6491.
[26] N.M. Dimitrijevic, P.V. Kamat, J. Phys. Chem. 97 (1993) 7623–7626.
[27] N. Revathi, P. Prathap, Y.P.V. Subbaiah, K.T.R. Reddy, J. Phys. D-Appl. Phys. 41 (2008).
[28] S.H. Yu, L. Shu, Y.S. Wu, J. Yang, Y. Xie, Y.T. Qian, J. Am. Ceram. Soc. 82 (1999) 457–460.
[29] Y. Li, J. Du, S. Peng, D. Xie, G. Lu, S. Li, Int. J. Hydrogen Energy 33 (2008) 2007–2013.
[30] D.W. Jing, L.J. Guo, J. Phys. Chem. B 110 (2006) 11139–11145.
[31] H. Jeong, T. Kim, D. Kim, K. Kim, Int. J. Hydrogen Energy 31 (2006) 1142–1146.
[32] Y. Huang, Y. Wei, L. Fan, M. Huang, J. Lin, J. Wu, Int. J. Hydrogen Energy 34 (2009) 5318–5325.
[33] N. Barreau, Sol. Energy 83 (2009) 363–371.
[34] R. Bayón, J. Herrero, Appl. Surf. Sci. 158 (2000) 49–57.
[35] L. Meahcov, I. Sandu, J. Fluoresc. 14 (2004) 181–185.
[36] N. Barreau, C. Deudon, A. Lafond, S. Gall, J. Kessler, Sol. Energy Mater. 90 (2006) 1840–1848.
[37] A. Lafond, C. Guillot-Deudon, S. Harel, A. Mokrani, N. Barreau, S. Gall, J. Kessler, Thin Solid Films 515 (2007) 6020–6023.
[38] A. Dickinson, D. James, N. Perkins, T. Cassidy, M. Bowker, J. Mol. Catal. A: Chem. 146 (1999) 211–221.
[39] M. Hara, J. Nunoshige, T. Takata, J.N. Kondo, K. Domen, Chem. Commun. 9 (2003) 3000–3001.
[40] A.L. Linsebigler, G.Q. Lu, J.T. Yates, Chem. Rev. 95 (1995) 735–758.
[41] D.E. Eastman, Phys. Rev. B 2 (1970) 1–2.